Effect of Alloying Element Partition in Pearlite on the Growth of Austenite in High-Carbon Low Alloy Steel

Z.N. YANG, Y. XIA, M. ENOMOTO, C. ZHANG, and Z.G. YANG

The growth of austenite from pearlite in high-carbon low alloy steel occurs with and without alloy element redistribution depending on the amount of superheating above the eutectoid temperature. The transition temperature of austenite growth (denoted PNTT) is calculated as a function of pearlite transformation temperature and subsequent holding time, which affect the degree of partitioning in pearlite, using experimental partition coefficients $k^{\theta/\alpha}$ of Mn, Cr, Co, Si, and Ni reported in the literature. PNTT is the highest in Cr-containing alloys which have the largest $k^{\theta/\alpha}$ in pearlite. Post-transformation aging, usually accompanied by cementite spheroidization, leads to a marked increase of PNTT in Mn and Cr alloys. PNTT of Ni alloy does not depend on pearlite transformation temperature because practically the formation of partitioned pearlite is severely limited in this alloy for kinetic reasons. Above PNTT, austenite growth occurs fast initially, but slows down in the order of ten seconds when the ferrite disappears, and the remaining small carbide particles dissolve very slowly under the control of alloy element diffusion.

DOI: 10.1007/s11661-015-3272-y
© The Minerals, Metals & Materials Society and ASM International 2015

I. INTRODUCTION

THE kinetics of austenitization from pearlite in high-carbon low alloy steel depends strongly on steel composition, *i.e.*, the species of alloying element.[1–4] Hillert[5] proposed two modes of austenite formation and cementite dissolution in alloy steel. At a low superheating above the eutectoid temperature, the long-range redistribution of alloy element is required, while above a certain critical temperature, the redistribution of alloy element is no longer necessary, and the growth of austenite occurs under carbon diffusion control. The diffusion of alloy element, if it occurs, is confined to a very narrow region ahead of the interface, which in effect maintains local equilibrium of alloy element at the interface. A similar transition occurs in the growth of proeutectoid ferrite from austenite; the long-range redistribution of alloy element between ferrite and austenite takes place at a small undercooling below Ae_3 which is called partition local equilibrium (PLE) mode.[6,7] Below a certain temperature, alloy element partition is not required, and the growth is controlled by carbon diffusion, which is called no-partition local equilibrium (NPLE) mode. Because the transformation temperature is often lower in ferrite transformation, the ferrite growth is thought to occur also under paraequilibrium in which the diffusion of alloy element is entirely suppressed.[8]

Xia *et al.*[9] calculated the transition temperature between the two modes of austenite growth, which they denoted partition-to-no-partition transition temperature (PNTT), in Fe-0.6 pctC-M alloys (M = Mn, Si, Cr, and Ni) and ascertained that PNTT and the growth rate varied widely with the species of alloy element. They assumed in the calculation that the pearlite formed at 923 K (650 °C) and alloy element partitioned to full equilibrium between pearlitic ferrite and cementite prior to austenitization. According to the literature, however, the extent of alloy element partitioning between ferrite and cementite is considerably dependent on pearlite transformation temperature, here designated T_{ptr}.[10–19] Equilibrium partitioning can be achieved only at a very small undercooling. Moreover, the extent of partitioning increases during post-transformation aging which usually is accompanied by cementite spheroidization. Indeed, the partitioning of Mn and Cr proceeds over a period of 10 hours,[12,13] while the Si partitioning between pearlitic ferrite and cementite proceeds quite rapidly behind the pearlite/austenite interface.[16]

In this report, the transition temperature from the alloy element diffusion-controlled to the carbon diffusion-controlled growth of austenite is calculated using experimental data on the partition coefficient $k^{\theta/\alpha}$ of alloy element in pearlite, which were reported in a number of high-carbon low alloy steels,[11–17] and the effect of nonequilibrium partitioning on the growth of austenite is discussed in terms of thermodynamic and kinetic properties of alloy elements. Furthermore, the

Z. N. YANG, Graduate Student, C. ZHANG, Associate Professor, and Z.G. YANG, Professor, are with the School of Materials Science and Engineering, Key Laboratory for Advanced Materials of Ministry of Education, Tsinghua University, Beijing 100084, P.R. China. Y. XIA, Graduate Student, is with the School of Materials Science and Engineering, Key Laboratory for Advanced Materials of Ministry of Education, Tsinghua University, and also Current Researcher at Wuchang Shipbuilding Industry Corp. Ltd., Wuhan 430060, P.R. China. M. ENOMOTO, Emeritus Professor, is with Ibaraki University, Hitachi 316-8511, Japan. Contact e-mail: masato.enomoto.fe6c7x@vc.ibaraki.ac.jp

Manuscript submitted February 12, 2015.
Article published online December 28, 2015

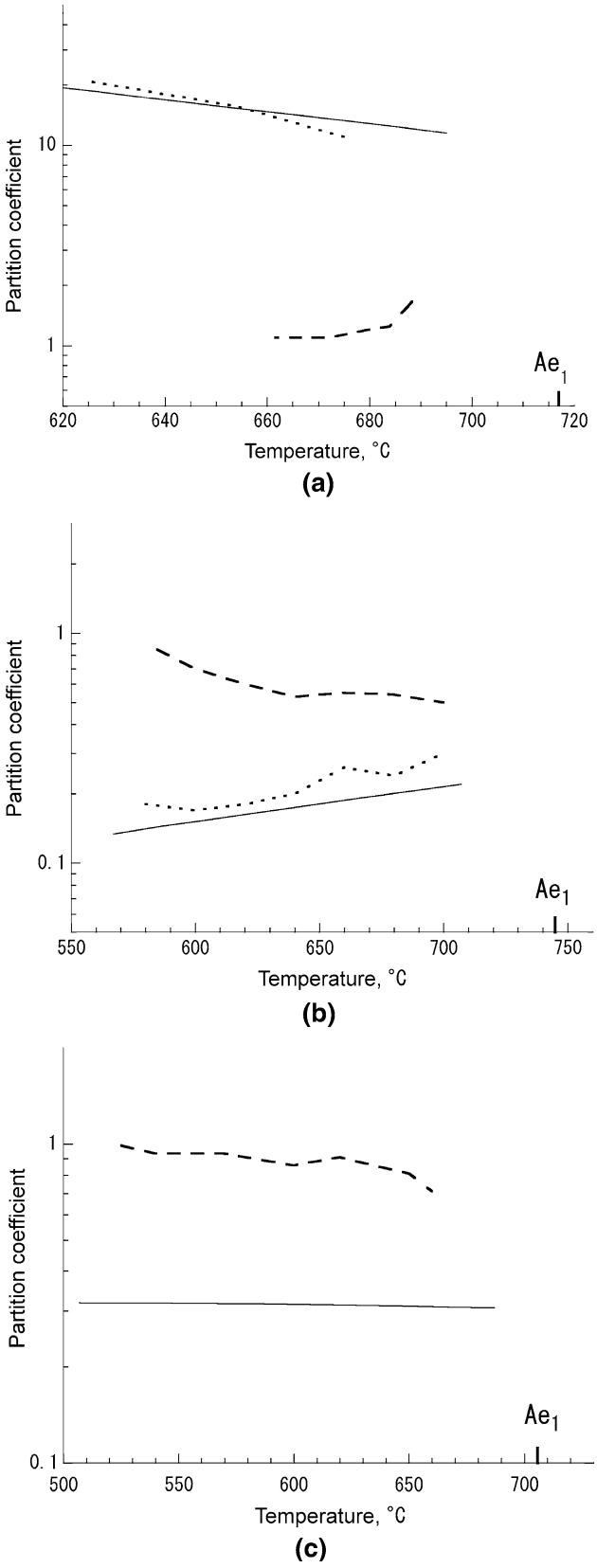

◀Fig. 1—Dependences of alloy element partition coefficients $k^{\theta/\alpha}$(start) (dashed curve) and $k^{\theta/\alpha}$(equil.) (dotted curve) on pearlite transformation temperature T_{ptr}, (*a*) in an Fe-0.80 pctC-1.08 pctMn alloy,[12] (*b*) in an Fe-0.82 pctC-2.20 pctCo alloy,[15] and (*c*) in an Fe-0.70 pctC-2.18 pctNi alloy.[17] Thin solid lines are equilibrium partition coefficients calculated from Thermo-calc.

growth of austenite which accompanies the shrinkage of ferrite and cementite is simulated to confirm the transition of growth behavior across PNTT. It will be seen that the kinetics of austenitization depends on not only prior microstructure,[20,21] but also on the composition of constituent phases provided by prior heat treatment.

II. ALLOY PARTITIONING IN PEARLITE TRANSFORMATION

A. *Summary of Data on Alloy Element Partitioning in Literature*

The alloy partitioning in pearlite has been studied extensively over the recent decades.[10,22] At earlier times, the concentrations of alloy elements were measured in thin foil and/or extraction replica using analytical electron microscope. The results are reported in the form of the partition coefficient defined by

$$k^{\theta/\alpha} = \frac{w^{\theta}}{w^{\alpha}} \qquad [1]$$

where w^{α} and w^{θ} are, respectively, the mass fractions of an alloy element in ferrite and cementite. Figure 1(a) illustrates schematically the variation of $k^{\theta/\alpha}$ of Mn with pearlite transformation temperature, in an Fe-0.80 pctC-1.08 pctMn alloy (in mass pct). The dashed line is the partition coefficient observed at the transformation front. It is denoted 'start' or 'interface' in the literature. Instead of direct measurement at the interface, it can be determined by extrapolating those measured in partially transformed specimens to the start time. The dotted line is the partition coefficient measured at prolonged holding which is denoted 'equilibrium.' A thin solid line was calculated from Thermo-Calc using TCFE7 database.[23] Even though $k^{\theta/\alpha}$(start) increases with T_{ptr} at the transformation front, $k^{\theta/\alpha}$(equil.) decreases with the increasing T_{ptr}. At a fixed temperature, $k^{\theta/\alpha}$(equil.) is greater than $k^{\theta/\alpha}$(start). This indicates that the partitioning proceeds during holding after transformation, which is usually accompanied by cementite spheroidization. The partitioning in Cr-containing alloys are similar to that of Mn alloys except that the absolute value of $k^{\theta/\alpha}$ is greater.[13,14] This is probably because Cr is an austenite stabilizer at the concentration less than several percent and the interaction with carbon is attractive and stronger than that of Mn, as seen from the Wagner interaction coefficient with carbon in austenite, see Table I.[24] The interaction between carbon and alloy element is thought to be qualitatively the same in ferrite and cementite as in austenite.

Figure 1(b) displays the dependence of $k^{\theta/\alpha}$ on T_{ptr} in an Fe-0.82 pctC-2.20 pctCo alloy.[15] Unlike Mn or Cr, the partition coefficient is less than unity: $k^{\theta/\alpha}$(start)

Table I. Wagner Interaction Parameter $\varepsilon_C^{(M)}$ in Austenite at 973 K (700 °C)[24]

Alloy Element	$\varepsilon_C^{(M)}$
Mn	−5.2
Cr	−15.1
Si	12.4
Co	2.9
Ni	5.6

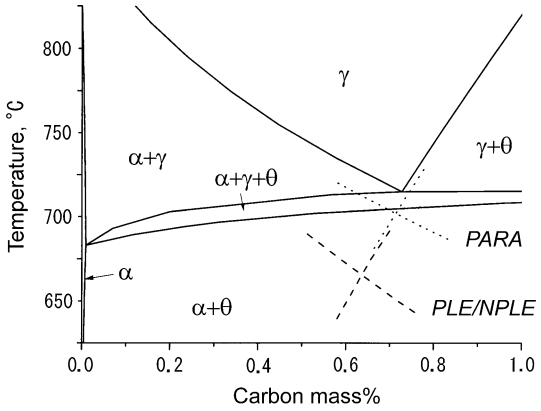

Fig. 2—Vertical section of Fe-C-Mn phase diagram calculated at 1.08 pctMn. Solid, dotted, and dashed lines show full equilibrium, paraequilibrium, and PLE (partition local equilibrium)/NPLE(no-partition local equilibrium) boundaries, respectively.

decreases and $k^{\theta/\alpha}$(equil.) increases with T_{ptr}, and $k^{\theta/\alpha}$(start) is greater than $k^{\theta/\alpha}$(equil.). This is because Co is repulsive with carbon and is enriched into ferrite. Si exhibits a similar behavior except that $k^{\theta/\alpha}$(equil.) is smaller than that of Co.[16] Figure 1(c) presents the temperature dependence of $k^{\theta/\alpha}$ (start) measured in an Fe-0.70C-2.18Ni alloy.[17] For the same reason equilibrium partitioning data are not available. Ni segregates in austenite at equilibrium with ferrite and cementite and is rejected from pearlite during growth. Since the diffusion of Ni is very slow in the austenite, the growth of pearlite accompanied by Ni partitioning is strongly suppressed.[25]

Figure 2 shows the eutectoid temperature and the ($\alpha + \gamma + \theta$) three-phase region of the 1.08 mass pctMn alloy calculated by Thermo-Calc. Two types of partitioned pearlite form depending on the amount of undercooling.[26,27] One is called divergent pearlite which forms at a small undercooling, *i.e.*, within the ($\alpha + \gamma + \theta$) three-phase region, in alloys of a relatively high concentration of Mn, Ni *etc.*[26] The lamellar spacing of divergent pearlite increases with the progress of transformation. The other is constant pearlite which forms below the ($\alpha + \gamma + \theta$) three-phase region, and grows with constant lamellar spacing. The overall composition of pearlite is identical to that of austenite, and thus, the fraction transformed can reach 100 pct. As shown later, *e.g.,* Figure 4(a), the reported partition coefficients were obtained below this temperature (open triangle therein) and thus belong to constant pearlite.

In the figure, paraequilibrium $\gamma/(\gamma + \alpha)$ and $\gamma/(\gamma + \theta)$ boundaries and PLE/NPLE boundaries of ferrite and cementite growth are included. The intersection of paraequilibrium $\gamma/(\gamma + \alpha)$ and $\gamma/(\gamma + \theta)$ boundaries corresponds to the thermodynamic upper limiting temperature of the formation of no-partitioned pearlite (parapearlite). On the other hand, the intersection of PLE/NPLE boundaries is the kinetic upper limiting temperature of no-partitioned pearlite. These boundaries can be compared with experimentally observed no-partition temperature. Since $k^{\theta/\alpha}$(start) varied gradually, Razik *et al.*[12] determined the critical temperature of paraferrite formation (henceforth denoted T_{para}) to be 956 K (683 °C) by plotting log $k^{\theta/\alpha}$ against $1/T$, where T *is* absolute temperature. This is located in the middle of the thermodynamic [975 K (702 °C)] and the kinetic upper limits [940 K (667 °C)] in Figure 2. Since $k^{\theta/\alpha}$ and $w^{\theta}$are still decreasing at 956 K (683 °C), T_{para} is a little lower than this and thus, may be closer to the kinetic upper limit, rather than the thermodynamic limit, in this alloy.

B. *Concentrations of Pearlitic Ferrite and Cementite*

In order to calculate the transition temperature, the alloy element concentrations in pearlitic ferrite (w^{α}) and cementite (w^{θ}) are necessary. They were calculated from reported $k^{\theta/\alpha}$ using the mass balance equation:

$$w^{\theta} f_{\theta} + w^{\alpha} f_{\alpha} = w^{0} \qquad [2]$$

where f_{α} and f_{θ} are the mass fractions of ferrite and cementite, and w^0 is the mass fraction of alloy element in the bulk.[12,14] The carbon concentrations in pearlitic ferrite and cementite vary with T_{ptr} by a small amount. Assuming that the carbon concentration in ferrite is 0.02 pct and taking the average of carbon concentration in cementite (~6.67 pct) over the possible range of w^{θ}, the mass fractions of ferrite and cementite were typically $f_{\alpha} = 0.88$ and $f_{\theta} = 0.12$, respectively.[13] w^{α} and w^{θ} were obtained in this way in all alloys except the 2.17Ni alloy in which w^{θ} itself was reported.[17]

C. *Calculation Procedure of Transition Temperature*

Figure 3(a) is a schematic illustration for austenite growth without the redistribution of alloy element, here assumed to be Mn, and Figure 3(c), for austenite growth accompanied by Mn diffusion. Open circles A and B represent the composition of pearlitic ferrite and cementite, respectively, prior to austenitization evaluated in the above procedure. Points a and b, connected by a carbon component ray (thin dashed line) to A and B, represent the compositions of austenite in the immediate vicinity of the γ/α and γ/θ interfaces, respectively. At a higher temperature T_1 (Figure 3(a)), the carbon activity in austenite at the γ/θ interface (denoted a_c^1) is greater than the carbon activity in austenite at the γ/α interface (a_c^2). Thus, carbon diffuses from the front of the

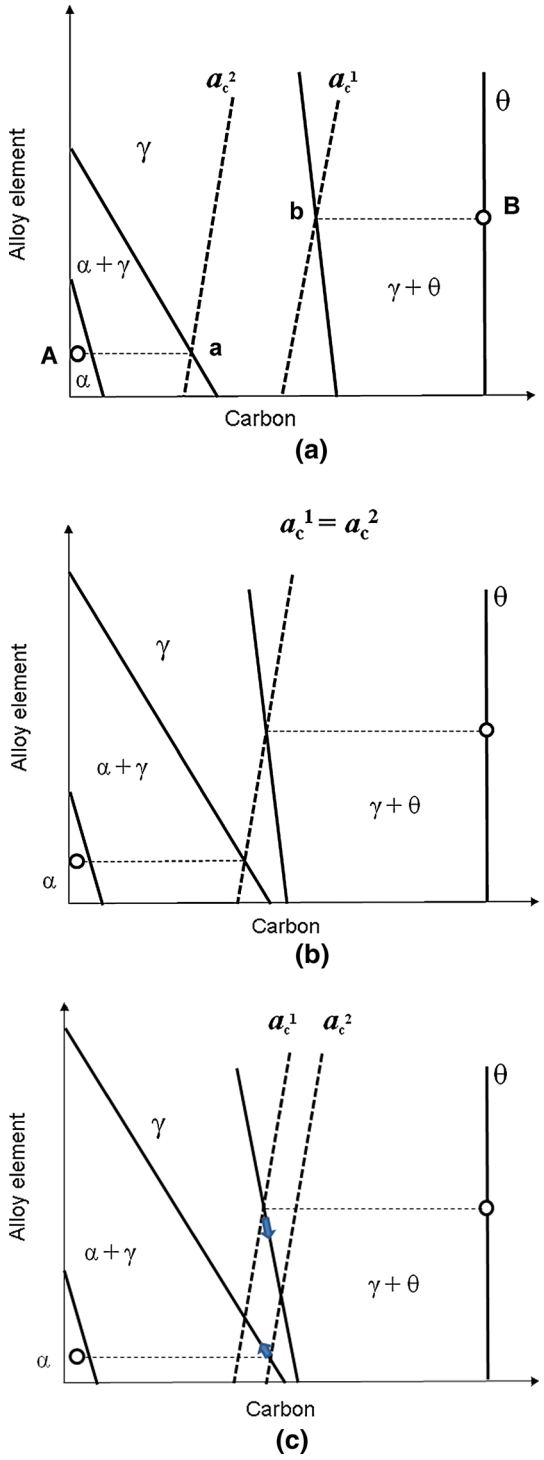

Fig. 3—Schematic illustration for the transition of austenite growth. (*a*) At a higher temperature (T_1), the austenite growth is controlled by carbon diffusion without the redistribution of alloy element. Circles A and B show the compositions of pearlitic ferrite and cementite, respectively. (*b*) The switching of growth mode occurs when the carbon activities a_c^1 and a_c^2 become equal. (*c*) At a lower temperature (T_2), the growth is controlled by alloy element redistribution.

cementite layer to the front of the ferrite layer, and the austenite can grow without Mn diffusion.[28] At a lower temperature T_2 (Figure 3(c)), a_c^1 is smaller than a_c^2. Thus, carbon does not diffuse toward the ferrite layer. The carbon flux toward the ferrite layer can occur only if the interfacial concentrations of Mn varied due to Mn diffusion as shown in the figure. The temperature at which a_c^1 and a_c^2 become equal (Figure 3(b)) is the lower limit of austenite growth without Mn redistribution.[9]

This temperature can be calculated following a similar procedure as the so-called secant method.[29] At first, T_1 and T_2 are selected by inspection. In the next step, a_c^1 and a_c^2 are calculated at $T_3 = (T_1 + T_2)/2$. If $a_c^2 < a_c^1$ at T_3, the transition temperature should lie between T_2 and T_3 and so forth. Repetition of this procedure several times would soon narrow the interval to less than one degree, and the sought temperature is accordingly obtained.

III. RESULTS

A. *Transition Temperature of Austenite Growth for Alloy Elements Which Segregate in Cementite*

In Figure 4(a), transition temperatures (PNTT) calculated from $k^{\theta/\alpha}$(start) and $k^{\theta/\alpha}$(equil.) are plotted against pearlite transformation temperature T_{ptr} in Fe-0.80 pctC-1.08 pctMn and Fe-0.69 pctC-1.80 pctMn alloys.[12] PNTTs under the 'start' (open circles and squares) and 'equil.' conditions (solid circles) exhibit similar dependence on T_{ptr} to that of $k^{\theta/\alpha}$ (Figure 1(a)). If the morphology change (spheroidization) does not occur, open circles and squares will merge with solid circles at Ae_1, where the growth of pearlite occurs infinitely slowly. T_{para}[= 922 K (649 °C)] of the 1.80 pctMn alloy is ~30 K lower than that of the 1.08Mn alloy. As will be discussed in Section IV–A, PNTT of parapearlite is equal to Ae_1 of the alloy, which is ~5 K lower in the higher Mn alloy. This is not the case for austenite growth from partitioned pearlite; PNTT calculated from $k^{\theta/\alpha}$ (equil.) at 923 K (650 °C) increased with the increasing Mn concentration.[9]

In Figure 4(b), the variation of PNTT with T_{ptr} was calculated in an Fe-0.81 pctC-1.41 pctCr alloy. Open and solid circles show a similar trend to those of Mn alloys except that PNTT is considerably higher.[30,31] The difference between the 'start' and 'equil.' conditions is also large. Figure 5 presents PNTT values calculated from $k^{\theta/\alpha}$ at various holding times in an Fe-0.82 pct-1.29 pctCr alloy,[13] which indicate the Cr enrichment in cementite and gradual increase of PNTT over 10 to 15 hours, giving rise to ~100 K difference between the as-transformed and aged (spheroidized) conditions. Since practically the alloy partitioning does not always occur homogeneously, a small difference in Cr partitioning may lead to a large scatter in the fraction of austenite in local areas.

B. *Transition Temperature of Austenite Growth for Alloy Elements Which Segregate in Pearlitic Ferrite*

Figures 6(a) and (b) show the calculated variations of PNTT with T_{ptr} in an Fe-0.84 pctC-1.94 pctSi and Fe-0.82 pctC-2.20 pctCo alloys, respectively. PNTT

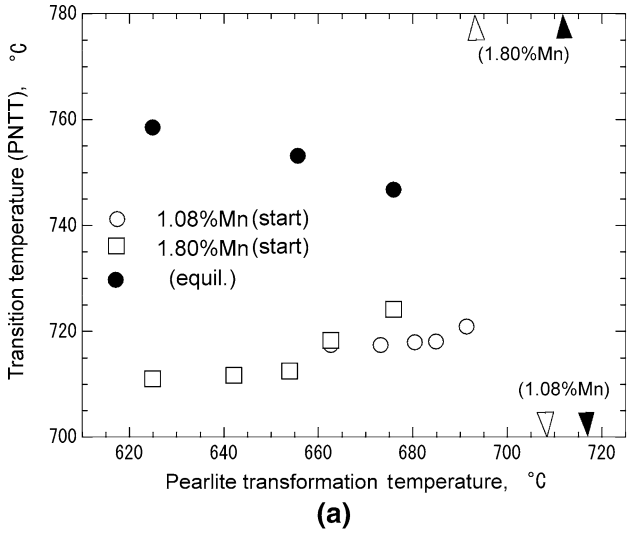

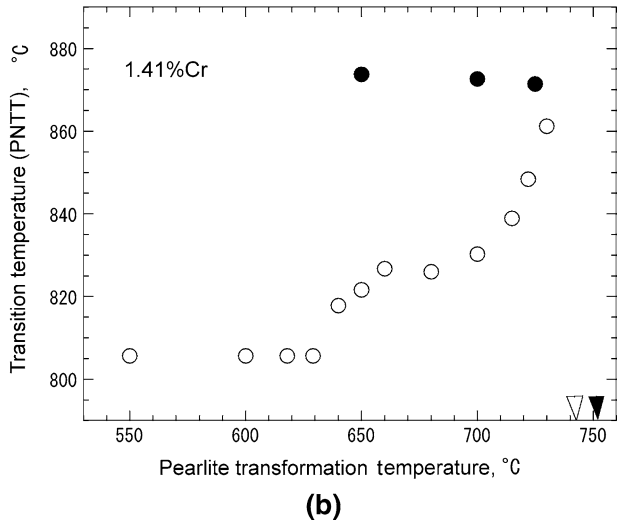

Fig. 4—Variations of PNTT with T_{ptr} calculated from $k^{\theta/\alpha}$(start) (open circles and squares) and $k^{\theta/\alpha}$(equil) (solid circles) a) in the 1.08 and 1.80 pctMn alloys. b) Variation of PNTT with T_{ptr} in an Fe-0.81 pctC-1.41 pctCr alloy.[14] Solid and open triangles indicate the Ae_1 and the phase boundary temperatures between the ($\alpha + \gamma + \theta$) three-phase and the ($\alpha + \theta$) two-phase regions.

calculated from $k^{\theta/\alpha}$(start) increased because the extent of partitioning increased with T_{ptr} (open circles). On the other hand, PNTT calculated from $k^{\theta/\alpha}$(equil.) does not vary significantly with T_{ptr} (solid circles). The differences between open and solid circles are much smaller than those of Cr or Mn alloys. Particularly, the variance in PNTT is less than a few degrees in the Co alloy.

In Figure 7, PNTT of an Fe-0.70 pctC-2.18 pctNi alloy is plotted against T_{ptr}. It is immediately seen that PNTT is almost independent of T_{ptr} over the temperature range encompassing the experimental no-partition temperature (T_{para} = 908 K (635 °C)[17]). In parapearlite, the Ni concentration is the same in pearlitic ferrite and cementite. At the eutectoid composition, the carbon activities of ferrite and cementite are identical. Hence, the eutectoid temperature Ae_1[= 978 K (705 °C)] is the transition temperature of austenite growth from

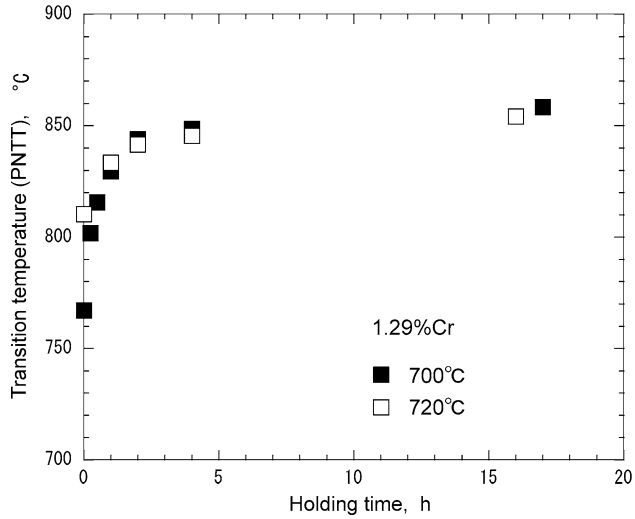

Fig. 5—Calculated variation of PNTT with holding time at 973 K and 993 K (700 °C and 720 °C) in an Fe-0.82 pctC-1.29 pctCr alloy.[13]

parapearlite. PNTT at two temperatures above T_{para} does not differ appreciably from those of parapearlite. This is because the extent of Ni partition is not large [$k^{\theta/\alpha} \sim 0.7$ at 933 K (660 °C)] and the C-Ni interaction is not strong (Figure 7).

IV. DISCUSSION

A. *Effects of Alloy Element on Transition Temperature*

Figures 8(a) and (b) show schematically how alloy elements partitioning in pearlite affects the transition temperature of austenite growth. For Mn and Cr which segregates in cementite, the gap between a_c^1 and a_c^2 lines is smaller under the 'equil.' condition than that under the 'start' condition (Figure 8(a)). The carbon activity at the γ/α interface in austenite a_c^2 may also differ between the 'start' and 'equil.' conditions. However, this was ignored for simplicity. In order to make a_c^1 and a_c^2 equal, the temperature must decrease. In decreasing temperature, the gap of 'equil.' will disappear first. Thus, PNTT calculated from $k^{\theta/\alpha}$(equil.) is higher than PNTT obtained from $k^{\theta/\alpha}$(start). For Co and Si which segregate in ferrite, the carbon activity a_c^2 is greater, and hence, the gap with a_c^1 is also narrower under the 'equil.' condition than that under the 'start' condition (Figure 8(b)). PNTT of 'equil.' is also higher for these elements. Thus, PNTT seems to increase with the extent of partitioning no matter whether the alloy element segregates in cementite or pearlitic ferrite. The variance of PNTT between the two conditions is smaller for Co which has weak interaction with carbon, see Table I. When the interaction with carbon is weak, the carbon isoactivity line is nearly vertical, and the gap between a_c^1 and a_c^2 becomes narrower between the 'start' and 'equil.' conditions.

Ni is unique in that PNTT calculated from $k^{\theta/\alpha}$(equil.) decreased with Ni concentration as discussed previously.[9] This implies that PNTT decreases with the extent

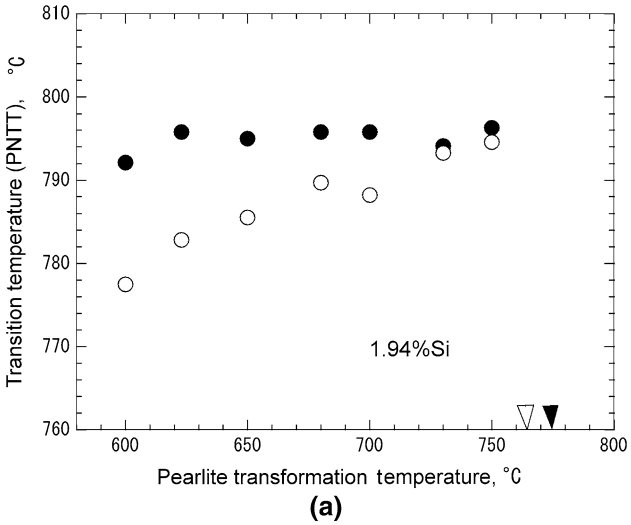

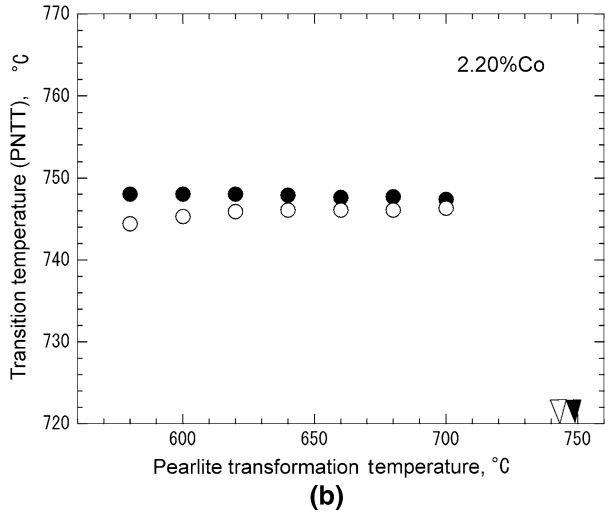

Fig. 6—Variations of PNTT with T_{ptr} calculated from $k^{\theta/\alpha}$(start) (open circle) and $k^{\theta/\alpha}$(equil) (solid circle) (*a*) in an Fe-0.84 pctC-1.94 pctSi alloy,[16] and (*b*) in the 2.20Co alloy.

of partitioning in contrast to other elements. This was not confirmed experimentally because the formation of partitioned pearlite is severely limited for kinetic reasons.

It was mentioned that PNTT of parapearlite is equal to the eutectoid temperature. All alloy elements except Al decreases the eutectoid temperature of high-carbon alloys no matter whether the alloy element segregates in ferrite or cementite.[32] Hence, PNTT of parapearlite in alloys containing Mn, Cr, and Ni will decrease with the increasing concentration. On the other hand, $k^{\theta/\alpha}$(equil.) does not vary significantly with alloy element concentration. Hence, the variation of PNTT with post-transformation holding time will increase with the concentration of alloy element.

B. *Simulation of Austenite Growth Above and Below the Transition Temperature*

To confirm the growth mode transition, austenite growth is simulated in the 1.08 pctMn and 1.80 pctMn alloys. It is assumed that in the 1.08 pctMn alloy, the

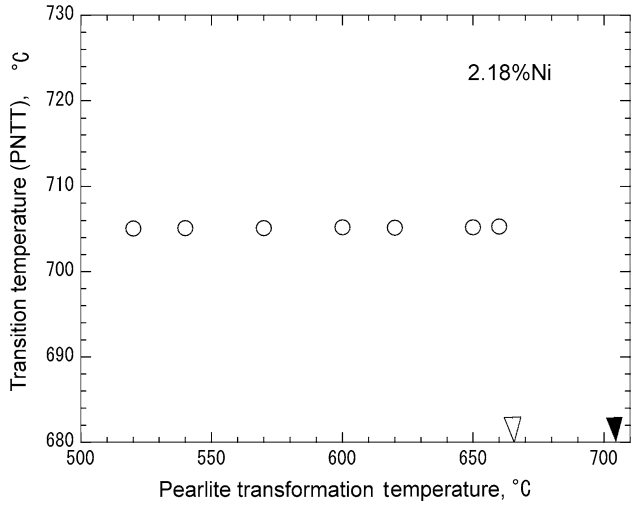

Fig. 7—Calculated variation of PNTT with T_{ptr} in the 2.18 pctNi alloy. T_{para} is 908 K (635 °C).

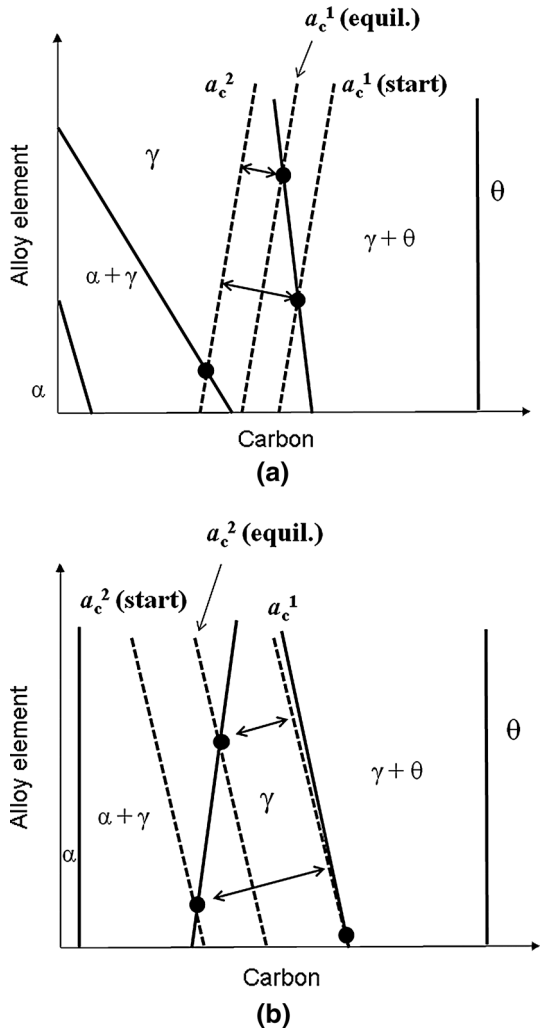

Fig. 8—Schematic illustration showing the gaps of the carbon activities at the γ/θ interface in austenite a_c^1 and the γ/α interface in austenite a_c^2 under the 'start' and 'equil.' conditions. (*a*) Alloy element which segregates in cementite, and (*b*) alloy element segregating in pearlitic ferrite.

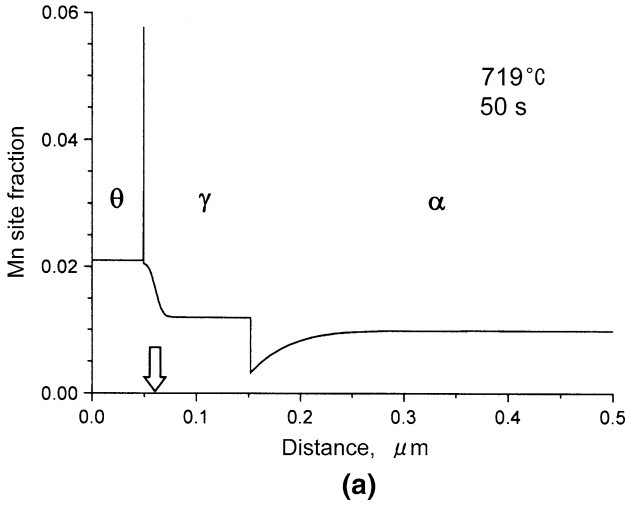

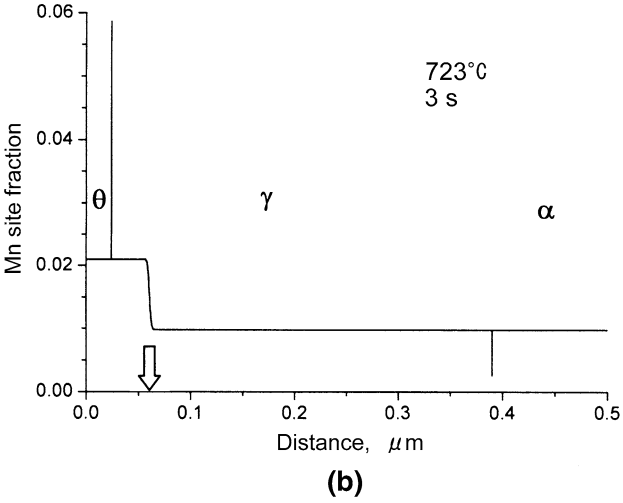

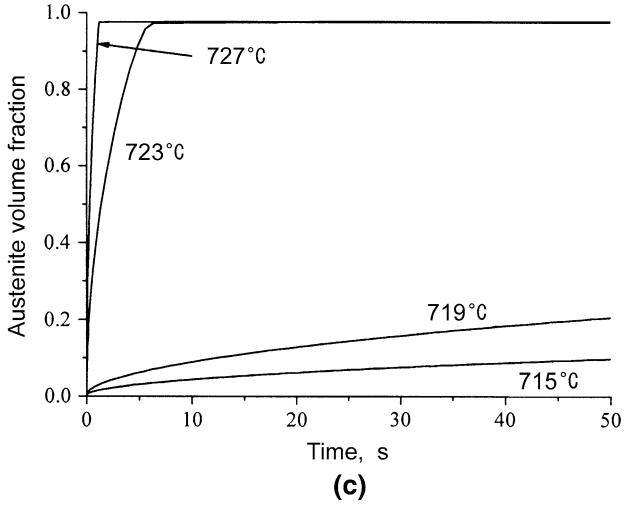

Fig. 9—Mn diffusion profile of austenite growth from lamellar pearlite (*a*) at 992 K (719 °C), and (*b*) at 996 K (723 °C) in the 1.08 pctMn alloy. The arrow indicates the initial position of θ/α interface. (*c*) The austenite volume fraction plotted against growth time calculated at four temperatures above and below PNTT [994 K (721 °C)] from $k^{\theta/\alpha}$(start).

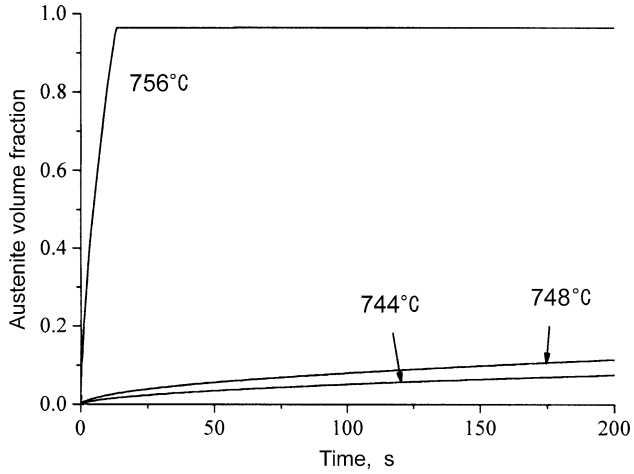

Fig. 10—Variation of austenite volume fraction with growth time in the 1.80 pctMn alloy calculated at three temperatures above and below PNTT (1023 K (750 °C) from $k^{\theta/\alpha}$ (equil.).

pearlite has formed at T_{ptr} = 965 K (692 °C) and PNTT is 994 K (721 °C). The thicknesses of ferrite and cementite layers are assumed to be 0.44 and 0.06 μm, respectively, from the reported lamellar spacing.[12] Figures 9(a) and (b) present the Mn diffusion profiles calculated 2 K below and above PNTT. In order to see the involvement of substitutional diffusion between the physically abutting phases, the diffusion profiles are plotted using the site fraction defined by $u_{Mn} = x_{Mn}/(1 - x_C)$, where x_{Mn} and x_C are the mole fractions of Mn and carbon, respectively. It is observed that below PNTT, Mn diffusion occurred in the region near both θ/γ and α/γ interfaces, whereas above PNTT, only thin Mn spikes are observed at the interfaces, and the overall Mn distribution is hardly altered to form a cliff of high Mn concentration within the austenite. The austenite volume fraction was plotted against growth time in Figure 9(c) at four temperatures. Evidently, the growth kinetics are markedly altered across PNTT of the alloy.

The transition of austenite growth also occurs in the spheroidized case. Figure 10 shows that the kinetics of austenite growth are markedly different below and above PNTT(= 1023 K (750 °C)) in the 1.80 pctMn alloy in which pearlite is assumed to have formed at T_{ptr} = 933 K (660 °C) and aged for a long time. The initial cementite radius and the diffusion cell size are assumed to be 1.0 and 2.1 μm, respectively.[12] It is noted that at 1029 K (756 °C), the austenite grows fast initially and the growth almost stops before the fraction transformed reaches 100 pct. To see this more closely, the volume fractions of austenite, ferrite, and cementite are plotted against holding time in Figures 11(a) through (c). It is seen that the fast austenite growth stops when the ferrite phase disappeared at $t \sim 13$ seconds. The initial fast dissolution of cementite also stops at a similar time, and the small residual part of cementite dissolves very slowly until it vanishes completely at $t \sim 6.5 \times 10^5$ seconds. This also happens in the lamellar

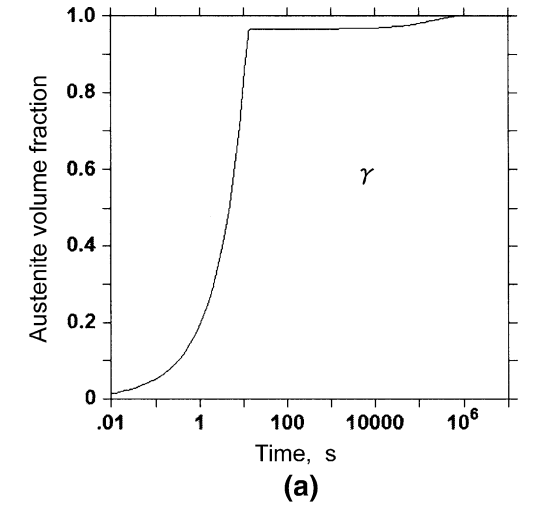

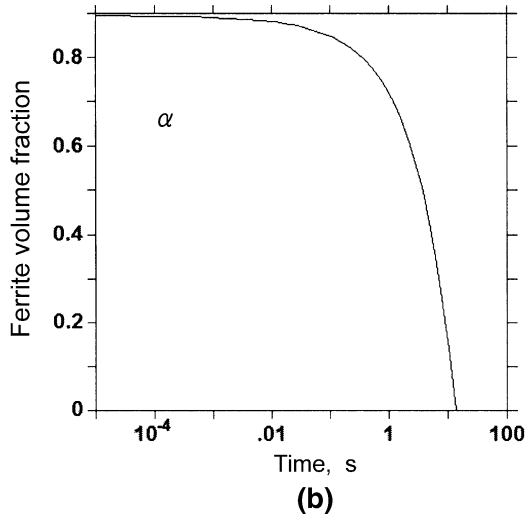

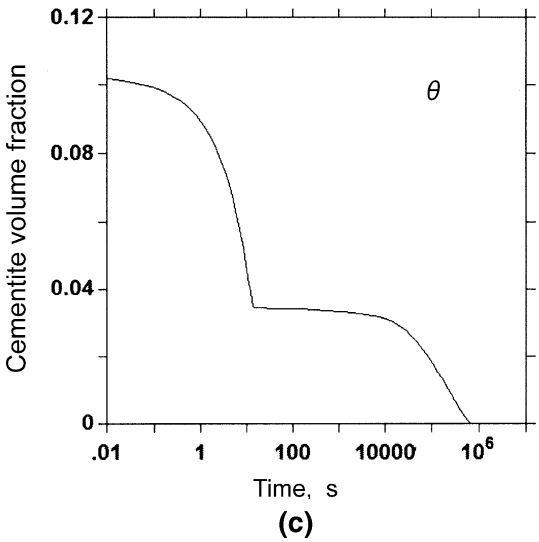

Fig. 11—Variations of (*a*) austenite, (*b*) ferrite, and (*c*) cementite volume fractions with time calculated at 1029 K (756 °C) (6 K above PNTT) in the 1.80 pctMn alloy.

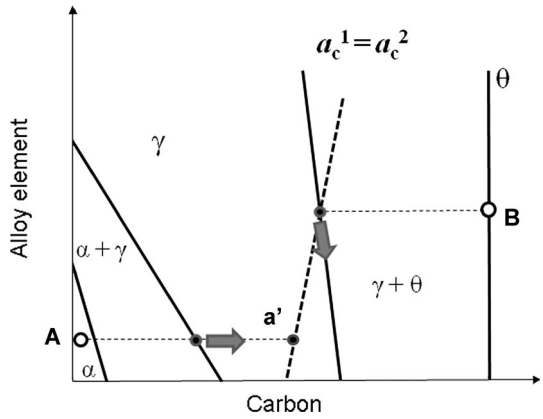

Fig. 12—Schematic illustration of the cessation of carbon diffusion-controlled growth of austenite and the onset of the growth accompanied by redistribution of alloy element.

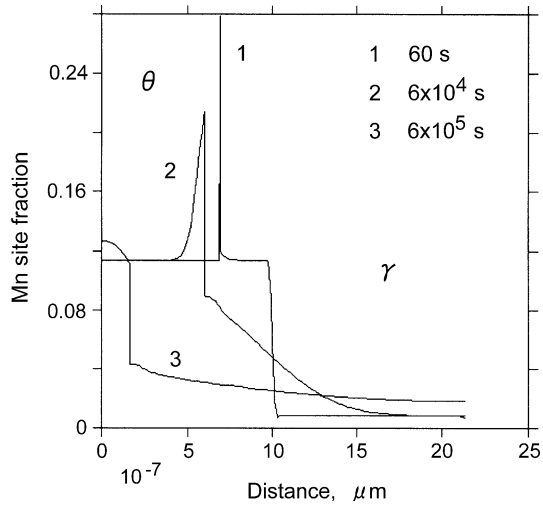

Fig. 13—Calculated evolution of Mn diffusion profiles at 1029 K (756 °C) after ferrite disappeared in the 1.80 pctMn alloy.

case (Figure 9(c)), in which the austenite fraction leveled off before it reached 100 pct. The retention of a small amount of cementite can be explained as follows. After the ferrite disappeared, the carbon concentration in austenite increases rapidly and soon reaches the point a' in Figure 12, at which the carbon activity at the γ/θ and γ/α interfaces are equal. In order to produce the gradient of carbon activity for further growth, the Mn concentration has to decrease along the $\gamma/(\theta + \gamma)$ boundary. The Mn diffusion profiles at very long times in Figure 13 indicate that this truly happened as the cliff of high Mn concentration collapses in austenite. A similar behavior was observed experimentally in the dissolution of carbide in austenite of Cr-containing alloys.[33,34] The period of initial fast carbide dissolution was less than a second,[35] considerably shorter than the period of fast growth of austenite (an order of 10 s). This is because the rate of increase of carbon concentration in the austenite is slow when the austenite region is expanding.

These results indicate that often small carbide particles remain when austenitization is carried out at a relatively low temperature. The residual carbide particles are thought to serve as nuclei of divorced eutectoid transformation when the alloy is cooled to immediately below Ae_1.[36] The cementite dissolution occurs predominantly edgewise in austenitization from lamellar pearlite, the retention of thin lamellar cementite has rarely been reported. Instead of thin layers a row of carbide particles, called pearlite ghost, is often observed.[37,38] This is because the high Mn concentration region remains for much longer time even after the θ/γ interface had vanished.

V. SUMMARY

The transition temperatures (PNTT) of austenite growth from pearlite with and without alloy element redistribution were calculated in near-eutectoid Fe-C-M alloys, where M is Mn, Cr, Si, Co, and Ni. Because the alloy element concentrations in pearlitic ferrite and cementite depend upon the pearlite transformation temperature and post-transformation aging time, the transition temperature is expected to vary with heat-treating conditions prior to austenitization. All elements except Ni increased PNTT with the increasing extent of partitioning. As a result, PNTT calculated from the partition coefficient $k^{\theta/\alpha}$ at prolonged holding time, during which cementite often is spheroidized, is always greater than that calculated from $k^{\theta/\alpha}$ measured at the transformation front. The transition temperature of carbide-forming element, *e.g.*, Mn and Cr, varies widely compared to those of ferrite-stabilizing element, *e.g.*, Si and Co. PNTT is highest in Cr alloys because of the large extent of enrichment in cementite.

PNTT of parapearlite is equal to the eutectoid temperature Ae_1 of the alloy. Thus, the dependence of PNTT of parapearlite on alloy element concentration is identical to that of Ae_1, which indicates that PNTT of parapearlite decreases with the increasing concentration of Mn, Cr, and Si. PNTT is practically constant in a Ni alloy of fixed content because partitioned pearlite hardly forms due to the kinetic constraint which operates during the growth of pearlite.

The growth of austenite varies by orders of magnitude across the transition temperature. When austenitization is carried out within a few tens of degrees above PNTT, the growth of austenite occurs fast initially and becomes sluggish after the ferrite disappeared. Small carbide particles remaining in the austenite often play a major role in the microstructural formation during the subsequent heat treatment.

ACKNOWLEDGMENTS

The support from the National Science Foundation of China (Grants 51471094) is gratefully acknowledged. M. Enomoto acknowledges the support on the Foreign Experts Recruitment Program of China Government.

REFERENCES

1. R.F. Mehl and W.C. Hagel: *Prog. Met. Phys.*, 1956, vol. 6, pp. 74–134.
2. G. Molinder: *Acta Metall.*, 1956, vol. 4, pp. 565–71.
3. R.R. Judd and H.W. Paxton: *Trans. TMS-AIME*, 1968, vol. 242, pp. 206–15.
4. G.R. Speich and A. Szirmae: *Trans. TMS-AIME*, 1969, vol. 245, pp. 1063–74.
5. M. Hillert, K. Nilsson, and L.E. Törndahl: *JISI*, 1971, vol. 209, pp. 49–66.
6. D.E. Coates: *Metal. Trans.*, 1972, vol. 3, pp. 1203–12.
7. D.E. Coates: *Metal. Trans.*, 1972, vol. 4, pp. 1077–86.
8. J.B. Gilmour, G.R. Purdr, and J.S. Kirkaldy: *Metall. Trans.*, 1972, vol. 3, pp. 1455–64.
9. Y. Xia, M. Enomoto, Z.G. Yang, Z.D. Li, and C. Zhang: *Phil. Mag.*, 2013, vol. 93, pp. 1095–09.
10. N. Ridley: In *Phase Transformations in Ferrous Alloys*, eds. A.R. Marder and J.I. Goldstein, TMS, Warrendale, PA, 1984, pp. 201–36.
11. M.L. Picklesimer, D.L. McElroy, T.M. Kegley, Jr, E.E. Stansbury, and J.H. Frye, Jr: *TMS-AIME*, 1960, vol. 218, pp. 473–80.
12. N.A. Razik, G.W. Lorimer, and N. Ridley: *Acta Metall.*, 1974, vol. 22, pp. 1249–58.
13. N.A. Razik, G.W. Lorimer, and N. Ridley: *Metall. Trans. A*, 1976, vol. 7, pp. 209–14.
14. J. Chance and N. Ridley: *Metall. Trans. A*, 1981, vol. 12, pp. 1205–13.
15. N. Ridley and D. Burgess: *Met. Sci.*, 1984, vol. 18, pp. 7–12.
16. S.A. Al-Salman, G.W. Lorimer, and N. Ridley: *Acta Metall.*, 1979, vol. 27, pp. 1391–1400.
17. S.A. Al-Salman and N. Ridley: *Scripta Metall.*, 1984, vol. 18, pp. 789–91.
18. S.A. Al-Salman, G.W. Lorimer, and N. Ridley: *Metall. Trans. A*, 1979, vol. 10, pp. 1703–09.
19. N. Ridley, M.A. Malik, and G.W. Lorimer: *Mater. Char.*, 1990, vol. 25, pp. 125–41.
20. A.E. Nehrenberg: *Trans. AIME*, 1950, vol. 188, pp. 162–74.
21. L. Karmazin: *Mater. Sci. Eng.*, 1991, vol. A142, pp. 71–77.
22. M.M. Aranda, R. Rementeria, J. Poplawsky, E. Urones-Garrote, and C. Capdevila: *Scripta Mater.*, 2015, vol. 104, pp. 67–70.
23. Thermo-calc is Trademark of Thermo-Calc Software: http://www.thermocalc.com/.
24. J.S. Kirkaldy, B.A. Thomson, and E.A. Baganis: In *Hardenability Concepts with Applications to Steel*, eds. D.V. Doane and J.S. Kirkaldy, TMS, 1978, pp. 82–125.
25. S.K. Tewari and P.C. Sharma: *Metall. Trans. A*, 1985, vol. 16, pp. 597–603.
26. M. Hillert: In *Solid → Solid Phase Transformations*, eds. H.I. Aaronson, D.E. Laughlin, R.F. Sekerka and C.M. Wayman, TMS, 1981, pp. 789–805.
27. C.R. Hutchinson, R.E. Hackenberg, and G.J. Shiflet: *Acta Mater.*, 2004, vol. 52, pp. 3565–85.
28. M. Gouné, P. Maugis, and J. Drillet: *J. Mater. Sci. Technol.*, 2012, vol. 28, pp. 728–36.
29. J.D. Faires and R.L. Burden: *Numerical Method*, PWS-KENT Publishing Company, Boston, 1993, pp. 32–33.
30. G. Miyamoto, H. Usuki, Z.D. Li, and T. Furuhara: *Acta Mater.*, 2010, vol. 58, pp. 4492–4502.
31. L. Kong, Y.H. Liu, J. Liu, Y. Song, S.S. Li, R.H. Zhang, T.J. Li, and Y. Liang: *J. Alloys Compd.*, 2015, vol. 648, pp. 494–99.
32. T. Nishizawa: *Bull. Japan Inst. Met.*, 1973, vol. 12, pp. 401–17.
33. J. Ågren and G.P. Vassilev: *Mater. Sci. Eng.*, 1984, vol. 64, pp. 95–103.
34. Z.K. Liu, L. Höglund, B. Jönsson, and J. Ågren: *Metall. Trans. A*, 1991, vol. 22, pp. 1745–52.
35. G.H. Zhang, J.Y. Chae, K.H. Kim, and D.W. Suh: *Mater. Sci. Eng.*, 2013, vol. 81, pp. 56–67.
36. J.D. Verhoeven and E.D. Gibson: *Metall. Mater. Trans. A*, 1998, vol. 29A, pp. 1181–89.
37. D.V. Shtansky, K. Nakai, and Y. Ohmori: *Acta Mater.*, 1999, vol. 47, pp. 2619–32.
38. Z.D. Li, G. Miyamoto, Z.G. Yang, and T. Furuhara: *Metall. Mater. Trans. A*, 2011, vol. 42A, pp. 1586–96.